Shahrekord University

Journal of Microfluidic and Nanofluidic Research

Journal homepage: https://jmnr.sku.ac.ir

Research Article

Numerical Study of the Impact of Fin Arrangement on Entropy Generation in a Mini-Channel Heat Sink

Ahmad Najafpour*

Department of Mechanical Engineering, Babol Noshirvani University of Technology, Babol, Iran

ARTICLE INFO

Article history:

Received: 2025-07-08
Revised: 2025-08-27
Accepted: 2025-08-29

Keywords:

Entropy Generation;
Reynols Number;
Thermal Management;
Geometric Parametrs.

ABSTRACT

This study numerically investigates the effect of fin arrangement on entropy generation and thermal performance in a heat sink subjected to a constant heat flux of 20 kW/m^2. Five different configurations are examined under laminar flow conditions within a Reynolds number (Re) range of 200–500. The analysis focuses on evaluating the contributions of fluid friction and heat transfer to the total entropy generation using a second-law approach. The results indicate that fin geometry and distribution significantly influence the thermodynamic behavior of the system. Increasing the Re intensifies viscous effects, leading to higher entropy generation due to fluid friction, while enhanced convection improves heat removal from the heated surface. Among the investigated configurations, Configuration 4 demonstrates the best overall performance. The larger number of fins in this configuration increases the effective contact area between the coolant and the solid surfaces, which enhances heat transfer and reduces overall entropy generation compared with the other cases.

1. Introduction

In recent years, the rapid evolution of electronic technologies toward more compact, faster, and higher-power devices has intensified the importance of effective thermal management in engineering applications [1,2]. The heat generated by electronic components directly influences their reliability and operational efficiency. Consequently, the development of efficient cooling strategies has become essential to prevent overheating and ensure stable device performance [3,4].

Traditional cooling techniques are increasingly insufficient for addressing the thermal demands of modern miniaturized and high-power electronic systems. To improve heat dissipation, several thermal management approaches have been investigated, including natural or forced air convection, liquid cooling methods, and advanced technologies such as phase change materials [5,6]. Although these solutions provide advantages in many situations, they often struggle to satisfy the strict thermal requirements of highly compact electronic devices. In this context, micro- and mini-channel heat sinks (MCHSs) have emerged as highly promising cooling solutions. Their compact geometry and high surface-to-volume ratio significantly enhance heat removal, particularly when liquid coolants are employed [7–9]. Due to these characteristics, MCHSs have been widely implemented in applications such as high-power electronic modules, solar energy equipment, and compact computing devices. Various working fluids, including water, oils, and ethylene glycolate commonly used, with liquid cooling generally offering superior performance because of stronger convective heat transfer mechanisms.

A considerable number of studies have focused on improving the performance of microchannel heat sinks by modifying channel geometry, introducing advanced working fluids,

* **Corresponding author.**
E-mail address: *amdnajafpour@gmail.com*

Cite this article as:

Najafpour, A. 2025. Numerical Study of the Impact of Fin Arrangement on Entropy Generation in a Mini-Channel Heat Sink. *Journal of Microfluidic and Nanofluidic Research*, 2(3), pp. 165-172. https://doi.org/10.22034/jmnr.2026.15052.1004

and developing hybrid thermal designs. For example, Gunnasegaran et al. [10] examined triangular, rectangular, and trapezoidal microchannels with different hydraulic diameters and reported that reducing the hydraulic diameter enhanced the heat transfer coefficient and improved temperature uniformity, while rectangular channels showed the best overall performance. Similarly, Najafpour et al. [11] investigated the impact of cross-sectional variations for Re between 831 and 1496 and observed that higher Re increased the heat transfer coefficient while lowering thermal resistance. Their study also indicated that incorporating nanoparticles such as TiO_2, MgO, and graphene oxide (GO) could enhance thermal performance by reducing both fluid temperature and overall thermal resistance compared with pure water. Ghadhban and Jaffal [12] analyzed microchannels with wave-shaped, S-shaped, and arc geometries, reporting improvements in the Nusselt number of up to 30.5% and a 16% reduction in pressure drop (ΔP) for the arc configuration. In another investigation, Al-Hassani and Freegah [13] explored serpentine microchannels with different secondary flow arrangements, including backward angles, dual outlets, and pin-fin hybrid structures. Their results demonstrated noticeable enhancements in the Nusselt number and overall hydrothermal performance, although changes in ΔP were also observed. Furthermore, Najafpour et al. [14] proposed multi-branch microchannel designs and evaluated their thermal behavior under a constant heat flux of 26.67 kW/m^2. Among the examined cases, Case 2 provided the most balanced performance between heat transfer improvement and flow resistance, with thermal resistance decreasing as the Re increased, while the ΔP simultaneously rose.

Despite considerable advancements in the development of microchannel heat sinks through geometric optimization and coolant enhancement, achieving a balanced trade-off between improved heat transfer and increased pressure loss continues to be a major challenge. Many proposed designs can significantly enhance heat dissipation; however, they often require higher pumping power, which limits their practicality in compact or energy-efficient electronic systems.

To address this gap, the present study proposes five fin-based configurations integrated into a copper heat sink. A constant heat flux = 20 kW/m^2 is applied to the bottom wall of the heat sink to evaluate the thermal performance of the proposed designs. The analysis is carried out over a Re range of 200–500, and a detailed entropy generation

2. Numerical methodology

2.1. Geometric dimensions and boundary conditions

In the present work, five distinct mini-channel heat sink configurations are developed and analyzed. The overall dimensions of the heat sink are 44 mm in length, 7 mm in width, and 4 mm in height. Each model consists of two solid copper sections and a fluid region through which water flows as the working fluid. The flow channel has a square cross-section with dimensions of 2 mm × 2 mm. The inlet temperature of the working fluid is set to 298 K, and a constant heat flux = 20 kW/m^2 is applied to the bottom wall of the heat sink (Fig. 1). The thermophysical properties of the materials used in the simulations are summarized in Table 1.

Table 1. Material Properties [3, 15]

Material	Water	Copper
ρ (kg/m3)	997	8933
c_p (J/kg.K)	4179	385
k (W/m.K)	0.6	401
μ (kg/m.s)	0.001	-

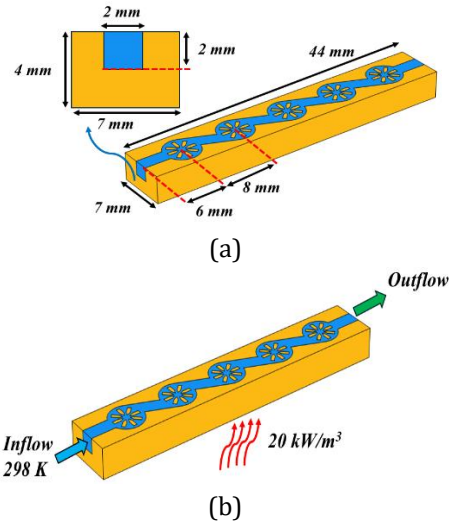

Fig. 1. (a) Geometric dimensions of the heat sink. (b)The boundary conditions.

The current designs include a single inlet with a hydraulic diameter of $D_h = 2$mm, through which the coolant enters the channel at a constant temperature. As the fluid flows through the channel, it absorbs heat from the heated surface and eventually leaves the system through an outlet located at the downstream end. The baseline model (Base Case) contains no fins, while Cases 1 to 4 are equipped with fins of

different geometric configurations in order to evaluate the impact of fin design on the cooling capability and overall thermal behavior of the heat sink (Fig. 2). The addition of fins modifies the flow structure and increases the effective heat transfer area, thereby promoting stronger convective heat transfer and improving temperature distribution within the system.

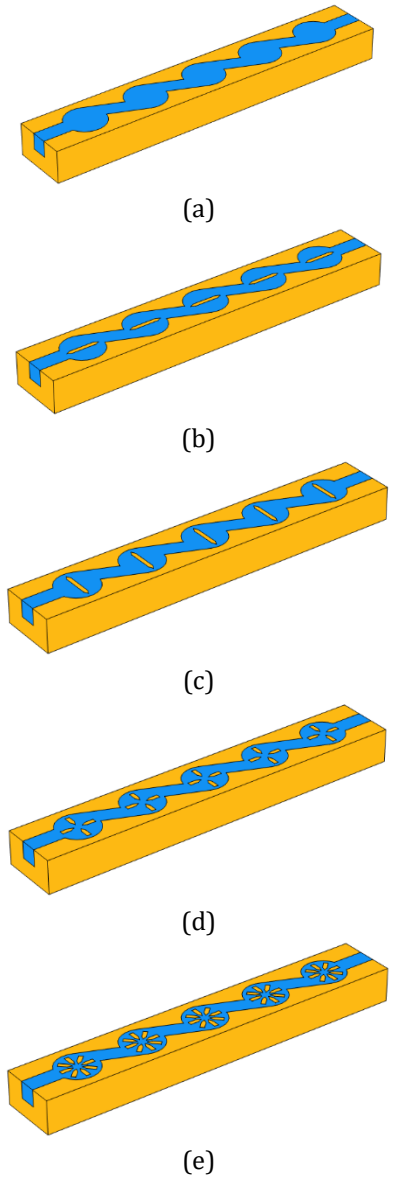

Fig. 2. Isometric view of: a) base case, b) case 1, c) case 2, d) case 3, and e) case 4

2.2. Governing equations

To develop a computational model that balances accuracy with computational efficiency, several simplifying assumptions are considered. These assumptions help reduce the complexity of the numerical analysis while still capturing the essential physical behavior of the system. The main assumptions adopted in this study are summarized as follows:

- The thermophysical properties of the materials are assumed to remain constant throughout the simulation and are not affected by temperature variations.
- The coolant flow is considered laminar and incompressible under the operating conditions examined.
- Gravitational effects and natural convection are neglected, allowing the analysis to focus exclusively on forced convection heat transfer.
- A uniform heat flux is applied to the bottom surface of the heat sink to represent a steady thermal load.
- Radiative heat transfer is assumed to be negligible and is therefore excluded from the model.

Based on these assumptions, the fluid flow and heat transfer within the computational domain are described using the fundamental conservation equations, including the continuity equation, the Navier–Stokes equations for momentum, and the energy equation.

The continuity equation is given as follows:

$$\frac{\partial u}{\partial x}+\frac{\partial v}{\partial y}+\frac{\partial w}{\partial z}=0 \quad (1)$$

Momentum equation:

X-momentum: $u\frac{\partial u}{\partial x}+v\frac{\partial u}{\partial y}+w\frac{\partial u}{\partial z}=-\frac{1}{\rho_f}\frac{\partial p}{\partial x}+\frac{\mu_f}{\rho_f}\left[\frac{\partial^2 u}{\partial x^2}+\frac{\partial^2 u}{\partial y^2}+\frac{\partial^2 u}{\partial z^2}\right]$ (2)

Y-momentum: $u\frac{\partial v}{\partial x}+v\frac{\partial v}{\partial y}+w\frac{\partial v}{\partial z}=-\frac{1}{\rho_f}\frac{\partial p}{\partial y}+\frac{\mu_f}{\rho_f}\left[\frac{\partial^2 v}{\partial x^2}+\frac{\partial^2 v}{\partial y^2}+\frac{\partial^2 v}{\partial z^2}\right]$ (3)

Z-momentum: $u\frac{\partial w}{\partial x}+v\frac{\partial w}{\partial y}+w\frac{\partial w}{\partial z}=-\frac{1}{\rho_f}\frac{\partial p}{\partial z}+\frac{\mu_f}{\rho_f}\left[\frac{\partial^2 w}{\partial x^2}+\frac{\partial^2 w}{\partial y^2}+\frac{\partial^2 w}{\partial z^2}\right]$ (4)

In this context, p, ρ and ν denote the pressure, density, and kinematic viscosity of the coolant, respectively. The energy equation for the fluid is formulated as follows:

$$u\frac{\partial T}{\partial x}+v\frac{\partial T}{\partial y}+w\frac{\partial T}{\partial z}=\frac{k_f}{\rho_f c_{pf}}\left[\frac{\partial^2 T}{\partial x^2}+\frac{\partial^2 T}{\partial y^2}+\frac{\partial^2 T}{\partial z^2}\right] \quad (5)$$

In this context, ρ, T, k_f and Cp denote the coolant's density, temperature, thermal conductivity, and specific heat at constant pressure, respectively.

Energy equation for the solid:

$$k_s\left[\frac{\partial^2 T}{\partial x^2}+\frac{\partial^2 T}{\partial y^2}+\frac{\partial^2 T}{\partial z^2}\right]=0 \quad (6)$$

where k_s is the thermal conductivity of the solid.

2.3. Data Analysis

The value of ΔP can be concluded as follows [16, 17]:

$$\Delta P = P_{in} - P_{out} \quad (7)$$

Re is defined as follows [18-20]:

$$Re = \frac{\rho V D_H}{\mu} \quad (8)$$

Where D_H represents the hydraulic diameter of the flow channel, which is calculated using the following equation [21, 22]:

$$D_H = \frac{4A}{P} \quad (9)$$

A denotes the cross-sectional area, and P represents the perimeter of the fluid inlet.

In this study, entropy generation analysis is utilized to evaluate the thermodynamic performance of the proposed MCHS configurations by quantifying the irreversibilities associated with heat transfer and fluid flow. This approach provides a comprehensive criterion for comparing different designs beyond conventional thermal indicators. The expressions used to calculate the total entropy generation rate are presented in the following section.

$$S_g = S_{g,\Delta p} + S_{g,\Delta T} \quad (10)$$

$$S_{g,\Delta p} = \frac{\dot{m}\Delta p}{\rho_m T_a} \quad (11)$$

$$S_{g,\Delta T} = \frac{Q_{base}\left(T_{base,avg} - T_a\right)}{T_{base,avg} T_a} \quad (12)$$

In this formulation, $S_{g,\Delta T}$ represents the entropy generation associated with heat transfer, whereas $S_{g,\Delta p}$corresponds to the entropy produced due to fluid flow effects. The fluid mass flow rate is denoted by $\dot{m}$, and the ambient temperature $T_a$is assumed to be equal to the inlet fluid temperature in the present analysis.

The augmented entropy generation number, $N_{s,a}$, is introduced as a useful parameter for comparing the level of thermodynamic irreversibility among different microchannel configurations. It can be expressed as follows [7, 8]:

$$N_{s,a} = S_g / S_{g,0} \quad (13)$$

In this relation, $S_g$corresponds to the total entropy generated in each configuration. The comparison between different cases is performed by relating their entropy generation to that of the baseline configuration through the parameter N_a. A smaller value of N_a indicates lower irreversibility within the system, which reflects a more efficient thermal management performance.

3. Grid Study and Validation

In CFD simulations, the accuracy of the numerical results is closely related to the quality of the computational mesh. Therefore, a mesh independence study was performed to confirm that the predicted results are not significantly affected by grid refinement. This process helps achieve a suitable balance between computational cost and solution accuracy, ensuring that the numerical results reliably represent the physical behavior of the system.

For this purpose, the grid independence analysis was carried out for Case 3 at a Re = 400, where key parameters such as ΔP and the heat sink base temperature were monitored. Several mesh densities were examined to evaluate their influence on the results. Based on the comparison, the Fine mesh was selected as the final computational grid since further refinement produced negligible changes in the obtained results (Table 2).

The governing equations of the present study were solved using the finite element method (FEM) implemented in COMSOL Multiphysics 6.2, where the equations were discretized and computed by considering all relevant boundary conditions and physical parameters.

Table 2. Mesh independence for case 3 at Re = 400

Mesh Size	Elements Number	ΔP (Pa)	Bottom Tem (K)
Coarse	518,935	441.78	300.21
Normal	951,712	479.11	300.35
Fine	**1,828,204**	**494.54**	**300.40**
Finer	2,734,131	496.38	300.42

To assess the reliability of the present numerical model, the simulation results were validated against the benchmark data reported by Al-Hasani and Freegah [13]. As illustrated in Fig. 4, the predictions obtained in this study exhibit good agreement with the results presented in the reference work, with only slight discrepancies observed.

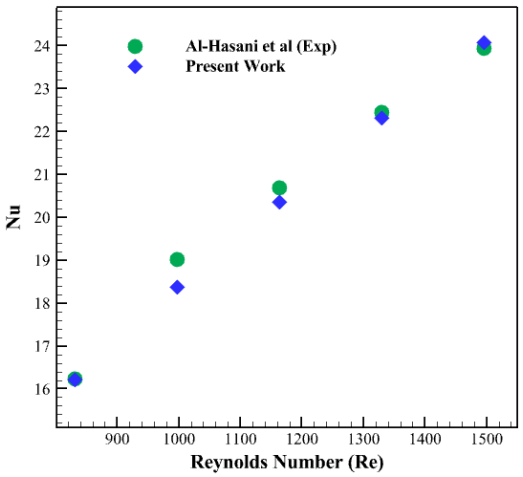

Fig. 3. Comparison of the results obtained with the current numerical method compared to the experimental study of Al-Hasani and Freegah [13].

4. Results and discussion

Figure 4 illustrates the temperature contour distributions at a Re = 400, providing insight into the heat dissipation behavior inside the heat sink. In the baseline configuration, relatively high-temperature regions are observed due to the limited heat transfer capability of the simple channel structure. However, when fins with different geometric arrangements are introduced in Cases 1–4, the temperature field becomes noticeably more uniform and the overall temperature level decreases. The presence of fins increases the effective heat transfer surface and improves the interaction between the coolant and the heated surfaces, which leads to enhanced convective heat transfer and better thermal management within the heat sink.

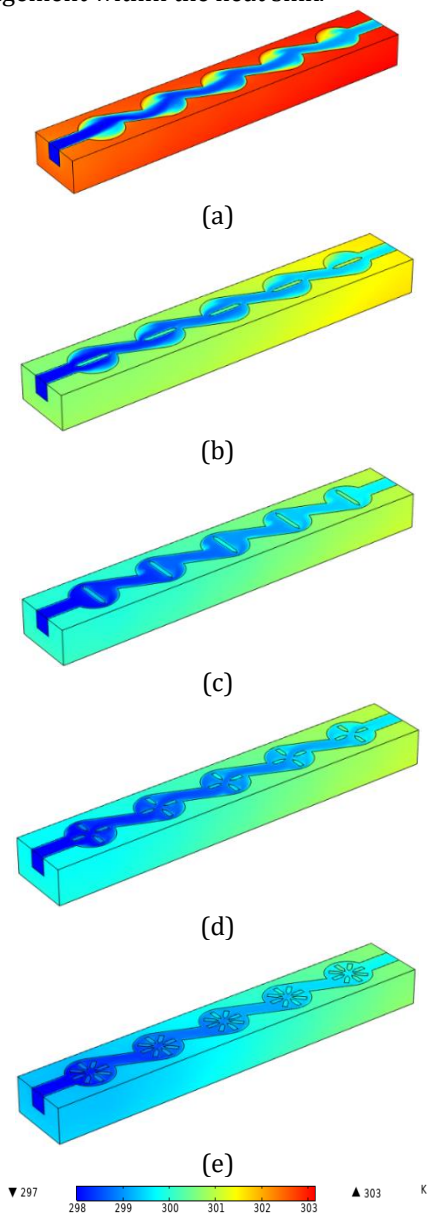

Fig. 4. Temperature distribution in present cases at a Re of 400: (a) base case, (b) case 1, (c) case 2, (d) case 3, (e) case 4.

Figure 5 illustrates the variation of entropy generation caused by fluid friction (Sp) as a function of the Re. As the Re increases, the fluid velocity inside the channel becomes higher, which intensifies the shear stress along the channel walls and consequently increases viscous dissipation. As a result, entropy generation associated with fluid friction rises for all examined configurations.

Nevertheless, the magnitude of Sp differs among the cases due to variations in fin geometry and their influence on the flow structure, boundary layer development, and local velocity gradients. The results indicate that the baseline configuration produces the lowest entropy generation, whereas Case 2 exhibits the highest values. In Case 2, fins are arranged perpendicular to the main flow direction, which forces the fluid to undergo abrupt changes in its flow path. This sudden redirection of the coolant increases flow resistance and ΔP, ultimately leading to higher entropy generation related to fluid friction.

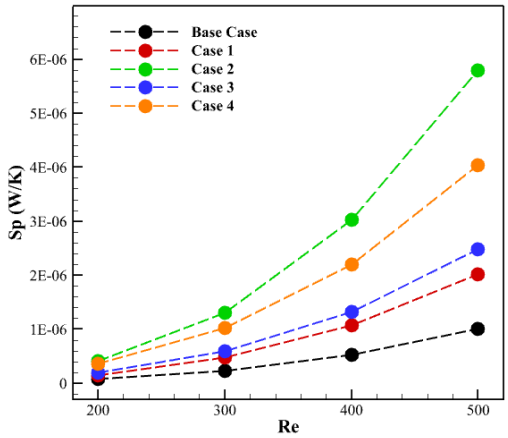

Fig. 5. S_p values for proposed cases at Re 200 to 500

Figure 6 presents the variation of entropy generation associated with heat transfer (S_t) for the proposed configurations within the Re range of 200–500. The results indicate that increasing the Re improves the cooling performance and overall heat transfer capability of the system. As the Re rises, the fluid velocity increases, which leads to a reduction in the thermal boundary layer thickness and enhances convective heat transfer between the coolant and the channel walls. Consequently, heat removal from the heated surface becomes more effective, and the temperature field inside the heat sink becomes more uniform.

The results also demonstrate that fin geometry plays a significant role in the thermal performance of the heat sink. Among the examined configurations, Case 4 exhibits the lowest values of S_t. This configuration contains the largest number of fins, which increases the contact surface area between the solid walls and the coolant. The enlarged heat transfer area strengthens convective cooling and results in lower entropy generation. At a Re = 300, the S_t

value in Configuration 4 decreases by 58.72% compared with the base case.

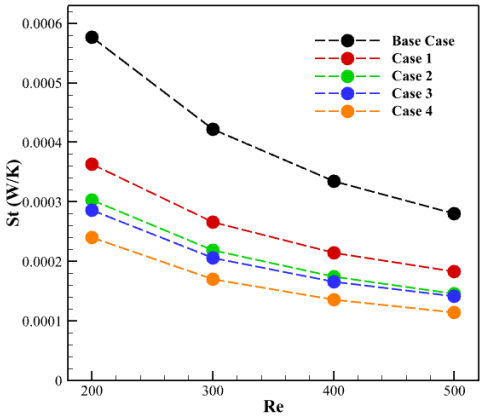

Fig. 6. S_t values for proposed cases at Re 200 to 500

Figure 7 illustrates the variation of the augmented entropy generation number (Na) for the proposed configurations compared with the baseline case over the Re range of 200–500. A lower value of Na indicates reduced thermodynamic irreversibility and therefore better performance from a second-law perspective. Consequently, configurations with smaller Na values are considered more efficient, as they reduce entropy generation and utilize the available energy more effectively within the heat sink.

5. Conclusions

In this work, five heat sink designs were analyzed under a uniform heat flux of 20 kW/m^2 to evaluate how different fin arrangements influence entropy generation and thermal behavior. The numerical simulations were carried out for laminar flow conditions within a Re range of 200–500. Particular attention was given to the role of fin distribution in modifying the interaction between the coolant flow and the heated solid surfaces.

The findings reveal that the configuration of fins significantly affects the thermodynamic performance of the heat sink. Among the studied designs, Configuration 4 delivers the most favorable performance according to the entropy generation principle. This configuration incorporates the highest number of fins, which expands the effective interface area between the fluid and the solid structure. As a result, heat transfer between the coolant and the heat sink is intensified, leading to a more efficient thermal management process with lower overall entropy production compared with the other configurations. The key outcomes of the present investigation are summarized below.

- At a Re = 300, the S_t value in Configuration 4 decreases by 58.72% compared with the base case.
- At Re = 200, Configurations 1 and 3 show improvements of 36.91% and 50.24%, respectively, compared with the baseline configuration.
- At Re = 500, the performance of Configurations 2 and 4 improves by 46.10% and 58.88%, respectively, relative to the base case.

The results show that fin geometry has a considerable influence on the thermodynamic performance of the system. Among the proposed designs, Configuration 4 exhibits the lowest Na values across the studied Re, indicating the best overall performance. At Re = 200, Configurations 1 and 3 show improvements of 36.91% and 50.24%, respectively, compared with the baseline configuration. Furthermore, at Re = 500, the performance of Configurations 2 and 4 improves by 46.10% and 58.88%, respectively, relative to the base case.

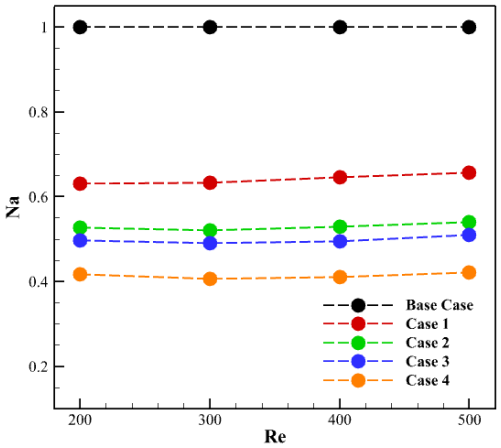

Fig. 7. N_a values for proposed cases at Re 200 to 500.

Nomenclature

Re	Reynolds Number
D_h	Hydraulic Diameter [m]
μ	Viscosity [Pa.s]
ΔP	Pressure Drop [Pa]
P	Pressure [Pa]
u	Velocity in x direction [m/s]
v	Velocity in y direction [m/s]
w	Velocity in z direction [m/s]
ρ	Density [kg/m^3]
c_p	Heat Transfer Capacity [J/kg.K]
k	Thermal Conductivity [W/m.K]
S_p	Entropy generation due to fluid flow (W/K)
S_t	Entropy generation due to heat transfer (W/K)

N_a Thermodynamic performance

References

[1] Ghazali, M. F., Maulana, M. I., Sidik, N. A. C., Najafi, G., Rashid, M. I. M., Jamlos, M. F., ... & Najafpour, A. (2024). Experimental analysis and CFD simulation of photovoltaic/thermal system with nanofluids for sustainable energy solution. *Journal of Advanced Research in Numerical Heat Transfer*, *24*(1), 1-13. https://doi.org/10.37934/arnht.24.1.113.

[2] Maulana, M. I., Ghazali, M. F., Abdullah, A., Che Sidik, N. A., Najafi, G., & Najafpour, A. (2024). Optimizing solar dish concentrator efficiency with nanofluids and diverse cavity design. *Journal of Advanced Research in Numerical Heat Transfer*, *25*(1), 87-99. https://doi.org/10.37934/arnht.25.1.8799.

[3] Najafpour A. Effect of Fin Geometry on Entropy Generation in Heat Sink: A Numerical Investigation. *Journal of Microfluidic and Nanofluidic Research*. https://doi.org/10.22034/jmnr.2025.15497.1018.

[4] Talebizadehsardari, P., Hosseinzadeh, K., Mohammed, H. I., Maarof, H. A., Rashid, F. L., Togun, H., ... & Cairns, A. (2026). Phase change materials in thermal management of Li-ion batteries: A state-of-the-art review. Journal of Energy Storage, 145, 119782. https://doi.org/10.1016/j.est.2025.119782.

[5] Parach, K., Jafari, B., & Hosseinzadeh, K. (2025). Numerical analysis of integrated photovoltaic thermal systems utilizing nanoparticles with phase change material and fin attachments. International Journal of Thermofluids, 27, 101210. https://doi.org/10.1016/j.ijft.2025.101210.

[6] Yasar, M., Hafsah, S., Juliaviani, N., Ghazali, M. F., Najafi, G., Rostami, M. H., & Najafpour, A. (2024). CFD Simulation of Solar Dish Concentrator with Different Cavity Receivers. Journal of Advanced Research in Numerical Heat Transfer, 25(1), 1-12. http://dx.doi.org/10.37934/arnht.25.1.112.

[7] Najafpour, A., Ranjbar, A. A., Ganji, D. D., & Hosseinzadeh, K. (2025). Entropy Generation and Thermal Analysis of Geometrically Modified Heat Sinks with Ternary Nanofluids. *Case Studies in Thermal Engineering*, 106713. https://doi.org/10.1016/j.csite.2025.106713.

[8] Najafpour, A., Hosseinzadeh, K., Hasibi, A., Ranjbar, A. A., & Ganji, D. D. (2025). Entropy Based Optimization of Mini-Channel Heat Sinks with Advanced Ternary Nanofluids for Photovoltaic Cells and Geometrical Enhancements. *Results in Engineering*, 104982. https://doi.org/10.1016/j.rineng.2025.104982.

[9] Najafpour, A., & Rostami, M. H. (2025). Numerical analysis of thermal and hydrothermal characteristics of a heat sink with various fin configurations and ternary nanofluid composition. *Case Studies in Thermal Engineering*, *68*, 105928. https://doi.org/10.1016/j.csite.2025.105928.

[10] Gunnasegaran, P., Mohammed, H. A., Shuaib, N. H., & Saidur, R. (2010). The effect of geometrical parameters on heat transfer characteristics of microchannels heat sink with different shapes. *International communications in heat and mass transfer*, *37*(8), 1078-1086.

[11] Najafpour, A., Hosseinzadeh, K., Kermani, J. R., Ranjbar, A. A., & Ganji, D. D. (2024). Numerical study on the impact of geometrical parameters and employing ternary hybrid nanofluid on the hydrothermal performance of mini-channel heat sink. *Journal of Molecular Liquids*, *393*, 123616. https://doi.org/10.1016/j.molliq.2023.123616.

[12] Ghadhban, F. N., & Jaffal, H. M. (2023). Numerical investigation on heat transfer and fluid flow in a multi-minichannel heat sink: Effect of channel configurations. *Results in Engineering*, *17*, 100839. https://doi.org/10.1016/j.rineng.2022.100839.

[13] Al-Hasani, H. M., & Freegah, B. (2022). Influence of secondary flow angle and pin fin on hydro-thermal evaluation of double outlet serpentine mini-channel heat sink. *Results in Engineering*, *16*, 100670. https://doi.org/10.1016/j.rineng.2022.100670.

[14] Najafpour, A., Montazer, E., Hosseinzadeh, K., Ranjbar, A. A., Ganji, D. D., & Kanesan, J. (2024). Computational study on the impact of geometric parameters on the overall efficiency of multi-branch channel heat sink in the solar collector. *International Communications in Heat and Mass Transfer*, *158*, 107884. https://doi.org/10.1016/j.icheatmasstransfer.2024.107884.

[15] Najafpour, A., Faraji, N., & Iji, F. (2025). T-Shaped Active Micromixer Analysis: AC Electric Field Effect. *Journal of Microfluidic and Nanofluidic Research*. https://doi.org/10.22034/jmnr.2025.15183.1013.

[16] Najafpour, A., Hosseinzadeh, K., Akbari, S., Mahboobtosi, M., Ranjbar, A. A., & Ganji, D. D. (2023). Numerical study of mixing performance in T-junction passive micromixer with twisted design. *Chemical Engineering and Processing-Process Intensification*, *194*, 109567. https://doi.org/10.1016/j.cep.2023.109567.

[17] Najafpour, A., Akbari, S., Hosseinzadeh, K., Bijarchi, M. A., Ranjbar, A. A., & Ganji, D. D. (2025). Active 3D electro-osmotic control micromixers: Effects of geometry, DC, and AC electric fields on mixing performance. International Communications in Heat and Mass Transfer, 165, 109033.

https://doi.org/10.1016/j.icheatmasstransfer.2025.109033.

[18] Bayareh, M., Alipour, F., Kharaji, Z. G., Sourani, S., Najafpour, A., & Bahrami, D. (2026). A critical review of micromixing dynamics in chemical microreactors. *International Communications in Heat and Mass Transfer*, *172*, 110739. https://doi.org/10.1016/j.icheatmasstransfer.2026.110739.

[19] Najafpour, A. (2026). Efficient electroosmotic mixing via DC and AC electric fields and novel geometric structure: A numerical approach. *International Communications in Heat and Mass Transfer*, *175*, 110957. https://doi.org/10.1016/j.icheatmasstransfer.2026.110957.

[20] Mahboobtosi, M., Hosseinzadeh, K., Najafpour, A., & Ganji, D. D. (2024). Entropy generation analysis of kerosene oil flow with ternary hybrid nanoparticles on the stretchable exponential surface. *International Journal of Modelling and Simulation*, 1-15. https://doi.org/10.1080/02286203.2024.2349506.

[21] Najafpour, A., & Bayareh, M. (2025). Influence of different electric fields on electroosmotic micromixing performance. *Chemical Papers*, 1-11. https://doi.org/10.1007/s11696-025-04333-9.

[22] Bayareh, M., & Najafpour, A. (2025). Mixing intensification of an electroosmotic micromixer with circular mixing units and constriction channels. *Chemical Engineering and Processing-Process Intensification*, 110557. https://doi.org/10.1016/j.cep.2025.11055.